
LidaRefer: Outdoor 3D Visual Grounding for Autonomous Driving with Transformers

Yeong-Seung Baek Heung-Seon Oh*

School of Computer Science and Engineering
Korea University of Technology and Education (KOREATECH)
{bys414, ohhs}@koreatech.ac.kr

Abstract

3D visual grounding (VG) aims to locate relevant objects or regions within 3D scenes based on natural language descriptions. Although recent methods for indoor 3D VG have successfully leveraged transformer-based architectures to capture global contextual information and enable fine-grained cross-modal fusion, they are unsuitable for outdoor environments due to differences in the distribution of point clouds between indoor and outdoor settings. Specifically, first, extensive LiDAR point clouds demand unacceptable computational and memory resources within transformers due to the high-dimensional visual features. Second, dominant background points and empty spaces in sparse LiDAR point clouds complicate cross-modal fusion owing to their irrelevant visual information. To address these challenges, we propose LidaRefer, a transformer-based 3D VG framework designed for large-scale outdoor scenes. Moreover, during training, we introduce a simple and effective localization method, which supervises the decoder's queries to localize not only a target object but also ambiguous objects that might be confused as the target due to the exhibition of similar attributes in a scene or the incorrect understanding of a language description. This supervision enhances the model's ability to distinguish ambiguous objects from a target by learning the differences in their spatial relationships and attributes. LidaRefer achieves state-of-the-art performance on Talk2Car-3D, a 3D VG dataset for autonomous driving, with significant improvements under various evaluation settings.

1 Introduction

3D visual grounding (VG) aims to locate objects or regions within 3D visual scenes guided by natural language descriptions. This task is crucial for enhancing interactions between humans and agents in various applications, such as autonomous driving, robotics, and VR/AR [4, 5, 31, 34, 36, 39]. In autonomous driving, precisely recognizing the locations of specific objects enables vehicles to make correct decisions based on human instructions. For example, in Fig. 1(a), 3D VG allows a vehicle to pinpoint a "gray car", guiding it to a designated parking spot.

Currently, most 3D VG research [14, 16, 18, 28, 33, 44, 46] has focused on indoor scenarios with various datasets [1, 2, 6, 47, 49] obtained through RGB-D cameras. Outdoor 3D VG is more challenging due to the extensive and sparse distribution of point clouds captured by LiDAR sensors and the frequent coexistence of objects in the same category as a target compared to indoor settings. To the best of our knowledge, MSSG [9] is a pioneering LiDAR-based outdoor 3D VG model for autonomous driving systems. However, it merely focuses on the correlation between a sentence-level text feature and distinct visual features for target identification, neglecting the meaning of

*Corresponding author

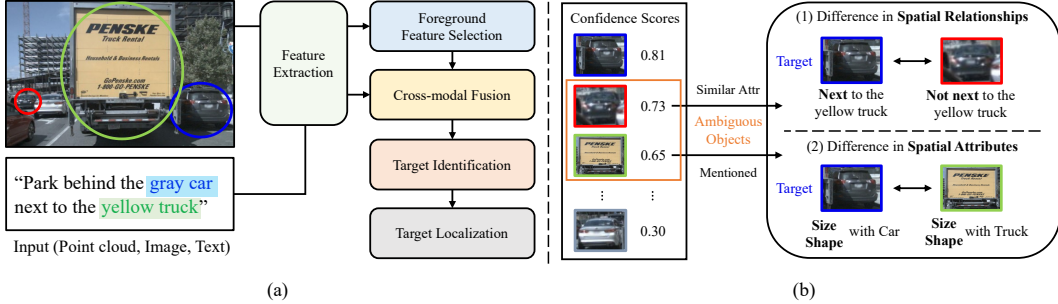


Figure 1: (a) Our transformer-based outdoor 3D VG framework utilizes 3D point clouds and RGB images as visual inputs, along with a language description as text input. (b) Some non-target objects can lead to ambiguity when they share attributes with the target or are mentioned in the description. The differences in their spatial relationships or attributes can distinguish these objects from the target.

individual words in a description and the contextual information among visual objects. This can lead to two issues: 1) When a description mentions multiple objects and attributes, a sentence-level text feature may not retain the specific meanings of individual words, failing to align adequately with corresponding visual features during cross-modal fusion. In Fig. 1(a), MSSG may incorrectly align visual features with the mentioned objects ("car" and "truck") and their colors ("gray" and "yellow"). 2) Furthermore, it also may struggle to identify the target "gray car", from two similar objects (red and blue circles) due to a lack of consideration for understanding the spatial relationship with "yellow truck" (green circle).

Recent indoor 3D VG models [20, 41] employ a transformer-based cross-modality encoder to effectively capture global contextual information within each modality and achieve the fine-grained alignment between word-level text features and their corresponding visual counterparts. Despite their effectiveness, directly applying this approach to outdoor 3D VG demands unacceptable computational and memory resources for processing high-dimensional visual features within transformers [37]. Even if feasible, the sparsity and dominance of background points in outdoor scenes can complicate cross-modal interactions due to their irrelevant visual information.

To this end, we propose **LidaRefer**, a transformer-based 3D VG framework, for autonomous driving in large-scale outdoor scenes. LidaRefer consists of five modular networks, as depicted in Fig. 1(a). Initially, visual and text data are encoded into deep features using separate modality encoders. Subsequently, inspired by recent 3D outdoor detectors [11, 32, 51], useful foreground features where objects are likely to occur are selected from high-dimensional visual features to efficiently retain a small number of relevant visual features. The selected visual and word features are fed into a transformer-based cross-modality encoder to capture contextual information and perform a fine-grained cross-modal alignment. Then, a target identification network determines a target query based on target confidence scores derived from cross-modal features. Finally, the target query is refined through interactions with the cross-modal features within the decoder to predict a 3D bounding box for the target object.

In VG scenarios, some non-target objects that exhibit similar attributes to the target or are mentioned in a description may be confused for the target, leading to ambiguity in target identification, as shown in Fig. 1(b). To deal with this, we introduce a simple and effective supervision method, **ambiguous object localization**, by considering the differences between the target and each type of ambiguous object. This method localizes both the target and some non-target objects that exhibit the highest confidence scores in target identification during training, thus enhancing an ability to distinguish ambiguous objects from the target by learning the differences derived from their spatial relationships or attributes within a scene.

Our contributions can be summarized as follows:

- We propose LidaRefer, a transformer-based 3D VG framework, to effectively understand global contextual information and facilitate cross-modal fusion in large-scale outdoor scenes for autonomous driving.

- We introduce a simple and effective localization method to distinguish ambiguous objects from the target by recognizing the differences in spatial relationships and attributes.
- We demonstrate LidaRefer’s superiority by achieving state-of-the-art results on Talk2Car-3D dataset and analyzing the effects under various evaluation settings.

2 Related Work

2.1 3D Visual Grounding

Currently, indoor 3D VG has attracted significant interest and advancement [14, 15, 16, 18, 19, 28, 29, 33, 44, 46], supported by various benchmark datasets [1, 2, 6, 47, 49]. In contrast, there are few methods for large-scale outdoor 3D VG. WildRefer [25] proposes both a model and dataset utilizing LiDAR point clouds, but it focuses solely on humans and covers a relatively narrow range (i.e., 30m radius). Unfortunately, the dataset has not been publicly available to researchers. Text2pos [23] and CityRefer [30] introduce 3D VG datasets with city-scale LiDAR point clouds and their baselines. However, they have a limitation that a point cloud must be divided into smaller subsets for processing within a single scenario. Several works [40, 48] have been developed for autonomous driving, but they only use RGB images as input visual data. To the best of our knowledge, MSSG [9] is a pioneering LiDAR-based 3D VG model for large-scale outdoor scenes. However, it encounters limitations due to its coarse-grained cross-modal fusion and lack of consideration for understanding contextual information.

2.2 Context-aware Modeling

Recognizing contextual information is crucial for accurate target identification in 3D VG tasks. Several methods [7, 38, 50] capture the spatial relationships among objects by utilizing the transformer’s attention mechanism. BUTD-DETR [20] effectively captures global contextual information and achieves fine-grained cross-modal alignment through its transformer-based cross-modal attention mechanism. Recent works [3, 20, 41] utilize the localization information of mentioned non-target objects to explicitly learn the specific contextual information between the target and these objects. While this approach offers potential benefits, it is limited in generalizability due to the necessity of manual processing steps, such as extracting mentioned objects from the description and their corresponding localization information. CORE-3DVG [43] proposes a pseudo-label self-generation method to extract contextual non-target objects efficiently. This approach is similar to our extraction strategy in that both automatically extract certain non-target objects to learn contextual information rather than relying on manual annotation. However, our method extracts the non-target objects based on target identification results, whereas CORE-3DVG uses cosine similarity between visual and text features regardless of target identification.

3 Method

3.1 Framework

Fig. 2 illustrates the overview of LidaRefer. It processes synchronized inputs comprising a point cloud and an RGB image (optional) as visual input and a language description as textual input. Although our goal is to predict a 3D bounding box for a target object referred to in the description, LidaRefer is supervised to localize both the target and ambiguous objects.

3.1.1 Feature Extraction

Visual Encoder There are two types of visual data: point clouds and images. In point cloud-only settings (LiDAR-only settings), points are encoded into visual features on the bird’s-eye-view (BEV) plane using a standard voxel-based 3D backbone [42], chosen for its proven efficiency and effectiveness in various outdoor detectors [35, 45, 51, 52]. In point cloud and image fusion settings (multimodal settings), we adopt Focals Conv’s [8] multimodal fusion strategy. Specifically, the 2D image features are extracted using a ResNet-50 [17] as a backbone to obtain texture information from an RGB image. Before converting to a BEV plane, each 3D voxel feature is matched with its corresponding 2D image feature using a 3D-to-2D projection and fused using a summation operation

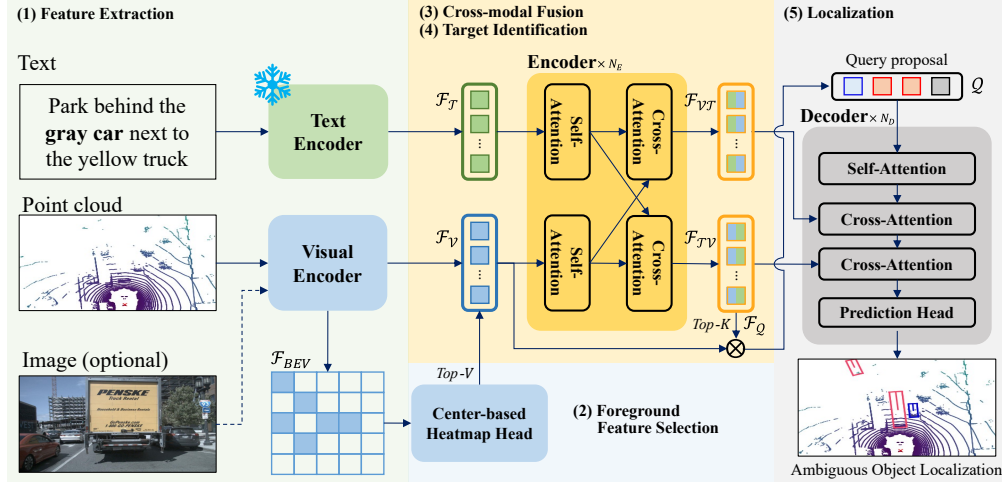


Figure 2: The overview of LidaRefer. After extracting visual and text features, useful foreground features are selected to reduce the number of visual features. Then, the visual and text features are fed into a transformer-based cross-modality encoder. Lastly, a target query, determined by a target identification network, is refined through a transformer-based decoder to predict a 3D bounding box for the target. During training, LidaRefer localizes some non-target objects within a scenario to alleviate ambiguity in target identification.

over the matched features. The generated texture-aligned 3D voxel features are converted onto a BEV plane in the same manner as in the LiDAR-only settings. Let $\mathcal{F}_{BEV} \in \mathbb{R}^{h \times w \times d}$ be the visual features, where h and w are the size of the BEV feature map and d is the number of hidden dimensions.

Text Encoder A language description is encoded into word-level text features using pre-trained RoBERTa [27], typically employed in other VG models [20, 21, 41, 48] as a text encoder, to leverage the prior knowledge about the words. Let $\mathcal{F}_T \in \mathbb{R}^{l \times d}$ be the text features, where l is the length of a description.

3.1.2 Foreground Feature Selection

Some transformer-based 3D VG models [20, 41] for indoor settings utilize all visual features containing the complete scene information as visual tokens in cross-modal fusion. Unfortunately, directly using the high-dimensional BEV features as visual tokens brings unacceptable computational and memory overheads in the attention layers of transformers. It forces the use of low-dimensional visual features but makes it challenging to capture small objects. Furthermore, it can lead to unstable learning in cross-modal fusion due to the irrelevant visual features generated from the background points dominating large-scale sparse point clouds.

Recent achievements in 3D outdoor detectors [11, 12, 13, 32, 51] have shown that foreground features are typically centered on objects within their high-dimensional feature representations. Inspired by this, useful foreground features are selected from BEV features to serve as visual tokens in our transformer-based cross-modality encoder to reduce computational and memory overheads. We follow the selection strategy used in CenterFormer [51]. A center heatmap head generates a C -channel heatmap $\mathcal{F}_{HM} \in \mathbb{R}^{h \times w \times c}$ for the centers of all objects, where each channel corresponds to one of C categories. The foreground features $\mathcal{F}_V \in \mathbb{R}^{v \times d} \subset \mathcal{F}_{BEV}$ are selected at the positions of top- V heatmap scores from the BEV features. It efficiently retains a small number of visual features highly related to objects, even for small ones, which enhances the capture of visual contextual information and facilitates fine-grained cross-modal alignment.

3.1.3 Cross-modal Fusion

In our transformer-based cross-modality encoder, visual and text tokens interact through N_E cross-modality encoding layers. Each encoding layer adds positional embeddings for the BEV plane and description to visual and text tokens, respectively. Then, the visual and text tokens perform

self-attention to capture the global contextual information of each modality and subsequently cross-attention to achieve fine-grained cross-modal alignment. As a result, we obtain text-aligned visual features $\mathcal{F}_{\mathcal{T}\mathcal{V}} \in \mathbb{R}^{v \times d}$ and visual-aligned text features $\mathcal{F}_{\mathcal{V}\mathcal{T}} \in \mathbb{R}^{l \times d}$, respectively.

3.1.4 Target Identification and Localization

As our decoder utilizes non-parametric queries generated from previously extracted features, determining initial queries from those features is crucial. Existing methods [20, 41] initialize query proposal features by selecting top- K features $\mathcal{F}_Q \in \mathbb{R}^{k \times d} \subset \mathcal{F}_{\mathcal{T}\mathcal{V}}$ based on target confidence scores computed by an MLP as a target identification head and then encoding \mathcal{F}_Q with a linear projection. However, such initialization from text-aligned visual features can pose challenges in box regression due to the potential degradation of objects’ pure visual information when aligned with text information within the cross-modality encoder. To preserve the original visual information, we extract and encode a subset of pure visual features from $\mathcal{F}_{\mathcal{V}}$ corresponding to the same position of \mathcal{F}_Q instead of directly encoding \mathcal{F}_Q .

3D bounding boxes are generated by updating the queries through N_D decoding layers. Within each decoding layer, positional embeddings for the BEV plane are added to query proposal features. Then, the queries self-attend to each other and sequentially cross-attend to $\mathcal{F}_{\mathcal{V}\mathcal{T}}$ and $\mathcal{F}_{\mathcal{T}\mathcal{V}}$. The refined queries are fed into a regression head to predict bounding boxes. At inference time, we use the box generated from the query with the top-1 highest target confidence score as the final prediction.

3.2 Ambiguous Objects Localization

In VG scenarios, an ambiguity problem in target identification arises due to two types of ambiguous objects. First, **attribute-similar objects** within the same category as the target object share characteristics such as size, shape, and color, leading to potential misrecognition. This issue is particularly critical in outdoor environments where many objects in the same category as the target coexist within a scene. Second, **contextual objects** referring to objects mentioned in a description but non-target might also be incorrectly perceived as the target if a model misinterprets the description. To address this problem, we should recognize the differences to distinguish these ambiguous objects from the target. As in Fig. 1(b-1), the differences in spatial relationships among visual objects should be recognized because attribute-similar objects are distinguished from the target by specifying the spatial relationships among mentioned objects in the description. Similarly, the differences in spatial attributes should be recognized because contextual objects, which typically belong to different categories from the target, possess distinct characteristics such as size and shape, as in Fig. 1(b-2).

Based on these insights, we propose a simple and effective localization method that simultaneously localizes the target and ambiguous objects. Our method recognizes the differences in spatial relationships and attributes through our transformer-based decoder. First, the queries learn the differences in spatial relationships through self-attention among themselves and cross-attention with both fused text and visual features after matching to target and ambiguous objects. Second, the differences in spatial attributes are learned by predicting the 3D bounding boxes for both target and ambiguous objects. Compared to the previous methods [3, 20, 41], mainly focusing on contextual objects, our method can capture more detailed contextual information owing to the inclusion of attribute-similar objects.

For this localization method, it is necessary to extract ambiguous objects and their annotated 3D bounding boxes within each scenario. However, such annotations are typically unavailable in practical applications, and even manually labeling them can be prohibitively expensive. Fortunately, annotated 3D bounding boxes for all objects in a scenario can be readily obtained using off-the-shelf 3D object detectors or manual annotations from object detection datasets, supersets of VG datasets. Exploiting this accessibility, we introduce an efficient annotation strategy to dynamically extract ambiguous objects and retrieve their annotated boxes from the complete set based on model prediction (i.e., confidence scores). Ambiguous objects often exhibit high confidence scores in target identification, leading to generating queries from their positions. Based on this observation, we construct a set of ambiguous objects \mathcal{A} for a scenario by applying a center-based object detector’s assignment strategy [45, 51] to all objects $\mathcal{O} = \{o_1, o_2, \dots, o_n\}$ within a scenario. This designates objects as ambiguous if they successfully match with the generated queries $\mathcal{Q} = \{q_1, q_2, \dots, q_k\}$. Formally, we define \mathcal{A} as:

$$\mathcal{A} = \{o \in \mathcal{O} \mid o \neq o_t \wedge \exists q \in \mathcal{Q} : \text{assign}(o, q) = \text{true}\} \quad (1)$$

Table 1: Two types of IoU threshold setting. "C.V." and "T.C." refer to construction vehicles and traffic cones, respectively.

Type	Car	Truck	C.V.	Bus	Trailer	Barrier	Motorcycle	Bicycle	Pedestrian	T.C.
A	0.5	0.5	0.5	0.5	0.5	0.25	0.25	0.25	0.25	0.25
B	0.7	0.7	0.7	0.7	0.7	0.5	0.5	0.5	0.3	0.3

where $\text{assign}(o, q)$ is an assignment function and o_t is the target object. This approach minimizes the labeling burden and enables the model to dynamically focus on ambiguous objects, continuously adapting to changing ambiguities as the learning progresses.

3.3 Loss Functions

LidaRefer is trained using a weighted sum of three different loss functions. First, in the foreground feature selection, a general heatmap classification loss \mathcal{L}_{hm} is used to supervise the center heatmap head to predict the center positions of all objects in a scene. Second, a target classification loss \mathcal{L}_{cls} is used to supervise the target identification network to predict a target query from text-aligned visual features. Third, a box regression loss \mathcal{L}_{reg} is used to supervise predicted boxes' center, size, and rotation. We adopt focal loss [26] for heatmap and target classification, and L1 loss for box regression. The final loss is defined as:

$$L = \lambda_1 L_{hm} + \lambda_2 L_{cls} + \lambda_3 L_{reg} \quad (2)$$

where the weights of three losses $\lambda_1, \lambda_2, \lambda_3$ are set to 1, 1, 1.25, respectively.

4 Experiments

Dataset. We evaluate LidaRefer on Talk2Car-3D derived from Talk2Car [10], a pioneering 2D VG dataset for autonomous driving, built upon nuScenes [4]. In establishing Talk2Car-3D, we follow the same preprocessing from MSSG [9] to convert 2D to 3D settings. Talk2Car-3D comprises 850 videos with multiple language descriptions. Each description deals with a single object, categorized into one of 23 categories. Talk2Car-3D is split into training, validation, and testing sets, comprising 7,115, 998, and 2,056 descriptions, respectively. As the foreground feature selection and ambiguous object localization require additional annotations (i.e., categories and bounding boxes) for non-target objects, not provided in Talk2Car, we obtain these annotations from the object detection dataset in nuScenes. During this process, we filter and utilize information only for non-target objects whose bounding box centers project onto the front camera images because the front camera perspective is only considered in Talk2Car.

Metric. $\text{Acc@IoU}_{\text{thr}}$ is used as an evaluation metric, where the predicted target box is considered correct if its 3D Intersection over Union (IoU) with the ground truth box exceeds a threshold. For a fair comparison to MSSG, we evaluate 10 super categories created by merging similar categories from 23 categories and set the same IoU thresholds as in Table 1. This threshold setting accounts for the significant variance in the size of objects in each category in outdoor environments, in contrast to indoor environments, where a uniform threshold is applied across all categories. Type-B is more challenging for localization than Type-A as it sets higher thresholds for all categories. If two models perform similarly in Type-A, a model outperforming in Type-B demonstrates superiority in object localization. In contrast, with similar results in Type-B, a model outperforming in Type-A reveals effectiveness in target identification.

Implementation details. We train LidaRefer for 20 epochs with a batch size of 4 on 4 Nvidia A6000 GPUs. Adam [22] optimizer using a one-cycle policy is used with a maximum learning rate of $4e-4$, a weight decay of 0.01, and a momentum from 0.85 to 0.95. After allocating the text and visual encoders, the same attention mechanism as [20, 41] is employed within our cross-modality encoder and decoder. The layers for the encoder and decoder are $N_E = 1$ and $N_D = 3$, respectively, while visual tokens v and proposal queries q are 500 and 256, respectively. The detection range is $[-54, 54]m$, $[0, 54]m$ and $[-5, 3]m$ for the X, Y, and Z-axes, respectively, and the voxel size is $(0.075m, 0.075m, 0.2m)$. We use two visual encoders based on the type of input visual data. In a LiDAR-only setting, a standard 3D voxel-based backbone [42] is used to extract 3D geometric information from point clouds. In a multimodal setting, in addition to the 3D backbone, ResNet-50

Table 2: Performance comparison on Talk2Car-3D. ‘-B’ and ‘-M’ denote our base and multimodal settings, respectively, while ‘-P’ denotes using pre-trained visual encoders.

Method	Pre-trained visual encoder	Validation		Test	
		A	B	A	B
<i>LiDAR-only setting</i>					
MSSG		31.9	20.3	-	-
MSSG-re		32.8	17.6	35.5	19.5
MSSG-Lida		35.2	22.4	38.7	22.6
LidaRefer-B (ours)		42.3	24.9	43.1	24.5
MSSG-P	✓	43.0	22.4	-	-
LidaRefer-P (ours)	✓	46.0	29.5	48.8	32.9
<i>Multimodal setting</i>					
LidaRefer-M (ours)		43.3	25.8	44.8	26.4
MSSG-MP	✓	45.4	23.7	-	-
LidaRefer-MP (ours)	✓	48.7	34.0	50.1	35.3

[17] pre-trained on MS-COCO [24], as a 2D backbone, is used to extract texture information from RGB images. We pretrain the visual encoders with 3D object detection task on nuScenes to acquire prior knowledge about the objects. To enhance model robustness against real-world variations, LidaRefer is trained with global scaling and translation augmentations applicable to both point clouds and RGB images.

Comparison Model. We use MSSG as our baseline model, a pioneering outdoor 3D VG model. To ensure a fair comparison and thorough validation, we construct two variants based on MSSG. First, we implement MSSG-Re, MSSG with the identical 3D visual and text encoder as LidaRefer. Second, we implement MSSG-Lida, an extension of MSSG-Re equipped with the foreground feature selection and ambiguous object localization, which are designed as flexible components for other outdoor 3D VG models.

4.1 Main Results

Table 2 compares the results of the comparison models across various configurations on Talk2Car-3D, where the top and bottom are for LiDAR-only and multimodal settings, respectively. In the LiDAR-only setting, LidaRefer consistently outperforms the comparison models in all configurations, underscoring the effectiveness of our context-aware framework and localization method. Specifically, LidaRefer-B, our base setting with a visual encoder trained from scratch, significantly outperforms MSSG in Type-A than Type-B. This highlights LidaRefer’s superior target identification capability in distinguishing targets from ambiguous objects by capturing global contextual information. LidaRefer-B also outperforms all configurations of MSSG in Type-B, demonstrating its superior localization ability. Surprisingly, LidaRefer-P, using a pre-trained visual encoder, obtains significant improvement in Type-B than Type-A, which contrasts with the results from MSSG. This suggests that prior knowledge about visual objects is more beneficial to localization than identification. In other words, LidaRefer-B exhibits stronger target identification capability than MSSG. In the multimodal setting, we achieve similar results, without exception, by incorporating image texture information.

The foreground feature selection and ambiguous object localization can be plug-and-play modules to boost existing 3D VG models. MSSG-Lida consistently outperforms MSSG-Re in all configurations, demonstrating the effectiveness and scalability of these proposed modules. However, despite these improvements, MSSG-Lida performs worse than LidaRefer-B because it is limited in understanding global contextual information and depends on a coarse-grained cross-modal fusion strategy that utilizes sentence-level text features.

4.2 Analysis

Effects of Selection and Localization. Tabel 3 explores the effectiveness of foreground feature selection and ambiguous object localization based on the ablations. To exploit all BEV features

Table 3: The ablation study of our proposed modules. ‘FFS’ and ‘AOL’ denote foreground feature selection and ambiguous object localization, respectively, while * denotes the increment of voxel size to exploit all BEV features as visual tokens.

Config	Voxel size	FFS	AOL	Validation		Test	
				A	B	A	B
LidaRefer-B	(0.075, 0.075, 0.2)	✓	✓	42.3	24.9	43.1	24.5
LidaRefer-B *	(0.15, 0.15, 0.2)	✓	✓	37.9	20.3	39.1	23.0
w/o foreground feature selection *	(0.15, 0.15, 0.2)		✓	36.1	19.5	37.5	22.0
w/o ambiguous object localization	(0.075, 0.075, 0.2)	✓		38.2	20.6	40.9	23.1
w/o both *	(0.15, 0.15, 0.2)			33.3	18.1	36.1	19.5

Table 4: Performance comparison of different localization methods. The major set, including Car, Truck, Bus, and Pedestrian, constitutes approximately 90% of the training dataset, while the minor set accounts for the remaining 10%.

Localized objects	Validation - A / B			Test - A / B		
	Major	Minor	Total	Major	Minor	Total
Target object (TO)	38.8 / 21.9	33.6 / 11.5	38.2 / 20.6	42.5 / 24.6	28.1 / 11.2	40.9 / 23.1
TO + All visible non-target objects	41.1 / 24.4	36.1 / 16.4	40.5 / 23.4	43.4 / 26.9	28.4 / 14.7	41.7 / 24.5
TO + Ambiguous non-target objects (LidaRefer-B)	42.4 / 26.3	41.0 / 18.9	43.2 / 24.9	44.5 / 25.8	32.3 / 14.7	43.1 / 24.5

as visual tokens without foreground feature selection, we increase the voxel size along the X and Y axes by a factor of two to reduce the resolution of the BEV feature map, which is maximally acceptable by the transformer within our GPU memory². When exploiting all BEV features as visual tokens during localizing ambiguous objects, a significant performance degradation occurs. This is due to the low-dimensional BEV features enforced by transformers, which struggle to detect small objects. Among them, excluding foreground feature selection has a more negative effect. We hypothesize that irrelevant visual features from dominant background points and empty spaces in LiDAR point clouds contribute to unstable cross-modal fusion learning, complicating target identification. Further, omitting ambiguous object localization while selecting foreground features, also results in a substantial performance drop but is relatively smaller than the former. This suggests that foreground feature selection is more critical than ambiguous object localization. The last row confirms the lower performance when both crucial components are absent.

Effects of Localization Methods. Table 4 investigates the effects of different localization methods tailored to the localized objects during training. To analyze the impact of category imbalance, we divided the categories into major and minor sets based on their frequency as targets. The results demonstrate that additional contextual information for non-target objects generally improves performance. Specifically, ambiguous non-target objects selected from all non-target objects are the most effective in Type-A. This suggests that focusing on the distinct differences between the target and ambiguous objects while excluding irrelevant non-target objects is more beneficial for target identification. Furthermore, the high performance in the minor set indicates that the model achieves a more comprehensive understanding of localization for objects within the minor set by learning to localize them even when they do not appear as targets.

Effects of Query Initialization. Table 5 investigates the effects of various query initialization strategies for non-parametric queries used as input in our decoder. As we expect, the text-aligned visual features outperform the positional embedding alone. Interestingly, the pure visual features achieve the best results. We hypothesize that the pure visual features preserve useful information about objects, whereas the text-aligned visual features lose it during the cross-modal fusion within the cross-modal encoder.

²GPUs with 48G memory are used.

Table 5: Performance comparison of different query feature initialization strategies.

Query initialization	Validation		Test	
	A	B	A	B
Positional embedding (PE)	33.1	14.9	32.7	13.0
PE + Text-aligned visual feature	38.1	23.0	42.0	24.5
PE + Pure visual feature (LidaRefer-B)	42.3	24.9	43.1	24.5

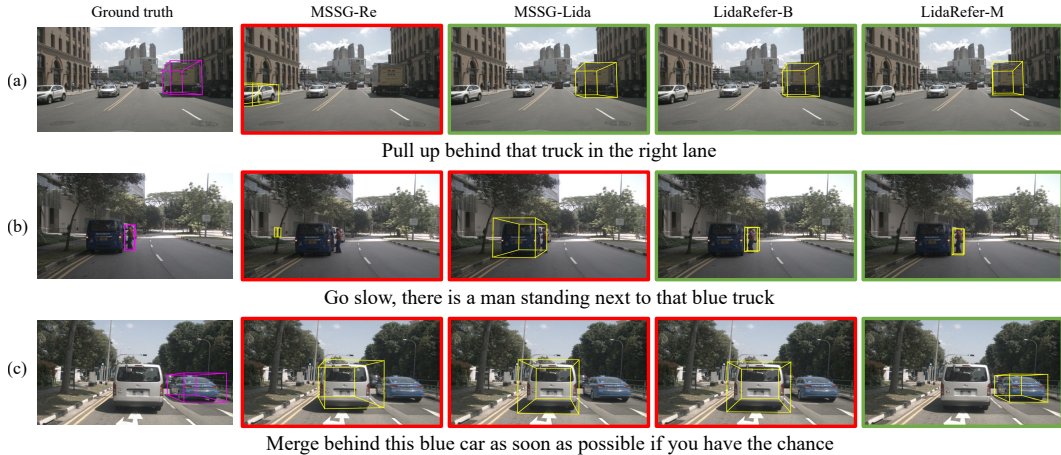


Figure 3: Visualization comparison from MSSG-based and LidaRefer-based methods for various scenarios. The ground truth and prediction boxes within the scenes are denoted in pink and yellow, respectively. Under Type-B of IoU threshold setting, the scenes in a green outline have correct predictions, whereas those in a red outline have incorrect ones.

4.3 Qualitative Results.

Fig. 3 illustrates the qualitative results from the variants of MSSG and LidaRefer. Fig. 3(a) shows that methods utilizing non-target object information in their training successfully identify the target object through their enhanced ability to distinguish different categories. Fig. 3(b) demonstrates that LidaRefer-based methods effectively understand contextual information in challenging scenarios where multiple objects within the same category as the target appear in a visual scene and a language description mentions multiple objects. In contrast, MSSG-based methods incorrectly identify non-target objects that either share a category with the target or are mentioned in the description. Fig. 3(c) shows that LidaRefer-M effectively utilizes RGB information for accurate target identification in scenarios where distinguishing the target based on color is essential.

5 Conclusion

This paper proposes LidaRefer, a 3D VG framework to effectively understand global contextual information and facilitate cross-modal alignment for advanced autonomous driving in large-scale outdoor scenes. Additionally, we introduce a new localization method to distinguish ambiguous objects from a target by recognizing the differences in their spatial relationships and attributes. Extensive experiments demonstrate the superiority of LidaRefer by comparing the strong baseline under various configurations on Talk2Car-3D.

References

- [1] A. Abdelreheem, K. Olszewski, H.-Y. Lee, P. Wonka, and P. Achlioptas. Scanents3d: Exploiting phrase-to-3d-object correspondences for improved visio-linguistic models in 3d scenes. *Proceedings of the IEEE/CVF Winter Conference on Applications of Computer Vision*, pages 3524–3534, 2024.

- [2] P. Achlioptas, A. Abdelreheem, F. Xia, M. Elhoseiny, and L. Guibas. Referit3d: Neural listeners for fine-grained 3d object identification in real-world scenes. *Computer Vision–ECCV 2020: 16th European Conference, Glasgow, UK, August 23–28, 2020, Proceedings, Part I 16*, pages 422–440, 2020.
- [3] E. M. Bakr, M. Ayman, M. Ahmed, H. Slim, and M. Elhoseiny. Cot3dref: Chain-of-thoughts data-efficient 3d visual grounding. *arXiv preprint arXiv:2310.06214*, 2023.
- [4] H. Caesar, V. Bankiti, A. H. Lang, S. Vora, V. E. Liong, Q. Xu, A. Krishnan, Y. Pan, G. Baldan, and O. Beijbom. nuscenes: A multimodal dataset for autonomous driving. *Proceedings of the IEEE/CVF conference on computer vision and pattern recognition*, pages 11621–11631, 2020.
- [5] C. Chen, U. Jain, C. Schissler, S. V. A. Gari, Z. Al-Halah, V. K. Ithapu, P. Robinson, and K. Grauman. Soundspaces: Audio-visual navigation in 3d environments. *Computer Vision–ECCV 2020: 16th European Conference, Glasgow, UK, August 23–28, 2020, Proceedings, Part VI 16*, 2020.
- [6] D. Z. Chen, A. X. Chang, and M. Nießner. Scanrefer: 3d object localization in rgb-d scans using natural language. *European conference on computer vision*, pages 202–221, 2020.
- [7] S. Chen, P. L. Guhur, M. Tapaswi, C. Schmid, and I. Laptev. Language conditioned spatial relation reasoning for 3d object grounding. *Advances in Neural Information Processing Systems*, 35, 2022. ISSN 10495258.
- [8] Y. Chen, Y. Li, X. Zhang, J. Sun, and J. Jia. Focal sparse convolutional networks for 3d object detection. *Proceedings of the IEEE/CVF Conference on Computer Vision and Pattern Recognition*, pages 5428–5437, 2022.
- [9] W. Cheng, J. Yin, W. Li, R. Yang, and J. Shen. Language-guided 3d object detection in point cloud for autonomous driving. *arXiv preprint arXiv:2305.15765*, 2023.
- [10] T. Deruyttere, S. Vandenhende, D. Grujicic, L. V. Gool, and M.-F. Moens. Talk2car: Taking control of your self-driving car. *arXiv preprint arXiv:1909.10838*, 2019.
- [11] L. Fan, F. Wang, N. Wang, and Z. Zhang. Fully sparse 3d object detection. *Advances in Neural Information Processing Systems*, 35, 2022. ISSN 10495258.
- [12] L. Fan, F. Wang, N. Wang, and Z. Zhang. Fsd v2: Improving fully sparse 3d object detection with virtual voxels. *arXiv preprint arXiv:2308.03755*, 2023.
- [13] L. Fan, Y. Yang, F. Wang, N. Wang, and Z. Zhang. Super sparse 3d object detection. *IEEE Transactions on Pattern Analysis and Machine Intelligence*, 45, 2023. ISSN 19393539. doi: 10.1109/TPAMI.2023.3286409.
- [14] M. Feng, Z. Li, Q. Li, L. Zhang, X. D. Zhang, G. Zhu, H. Zhang, Y. Wang, and A. Mian. Free-form description guided 3d visual graph network for object grounding in point cloud. *Proceedings of the IEEE International Conference on Computer Vision*, 2021. ISSN 15505499. doi: 10.1109/ICCV48922.2021.00370.
- [15] Z. Guo, Y. Tang, R. Zhang, D. Wang, Z. Wang, B. Zhao, and X. Li. Viewrefer: Grasp the multi-view knowledge for 3d visual grounding. *Proceedings of the IEEE International Conference on Computer Vision*, 2023. ISSN 15505499. doi: 10.1109/ICCV51070.2023.01410.
- [16] D. He, Y. Zhao, J. Luo, T. Hui, S. Huang, A. Zhang, and S. Liu. Transrefer3d: Entity-and-relation aware transformer for fine-grained 3d visual grounding. *MM 2021 - Proceedings of the 29th ACM International Conference on Multimedia*, 2021. doi: 10.1145/3474085.3475397.
- [17] K. He, X. Zhang, S. Ren, and J. Sun. Deep residual learning for image recognition. *Proceedings of the IEEE Computer Society Conference on Computer Vision and Pattern Recognition*, 2016-December, 2016. ISSN 10636919. doi: 10.1109/CVPR.2016.90.
- [18] P. H. Huang, H. H. Lee, H. T. Chen, and T. L. Liu. Text-guided graph neural networks for referring 3d instance segmentation. *35th AAAI Conference on Artificial Intelligence, AAAI 2021, 2B*, 2021. ISSN 2159-5399. doi: 10.1609/aaai.v35i2.16253.

- [19] S. Huang, Y. Chen, J. Jia, and L. Wang. Multi-view transformer for 3d visual grounding. *Proceedings of the IEEE Computer Society Conference on Computer Vision and Pattern Recognition*, 2022-June, 2022. ISSN 10636919. doi: 10.1109/CVPR52688.2022.01508.
- [20] A. Jain, N. Gkanatsios, I. Mediratta, and K. Fragkiadaki. Bottom up top down detection transformers for language grounding in images and point clouds. *European Conference on Computer Vision*, pages 417–433, 2022.
- [21] A. Kamath, M. Singh, Y. LeCun, G. Synnaeve, I. Misra, and N. Carion. Mdetr - modulated detection for end-to-end multi-modal understanding. *Proceedings of the IEEE International Conference on Computer Vision*, 2021. ISSN 15505499. doi: 10.1109/ICCV48922.2021.00180.
- [22] D. P. Kingma and J. L. Ba. Adam: A method for stochastic optimization. *3rd International Conference on Learning Representations, ICLR 2015 - Conference Track Proceedings*, 2015.
- [23] M. Kolmet, Q. Zhou, A. Ošep, and L. Leal-Taixé. Text2pos: Text-to-point-cloud cross-modal localization. *Proceedings of the IEEE/CVF Conference on Computer Vision and Pattern Recognition*, pages 6687–6696, 2022.
- [24] T. Y. Lin, M. Maire, S. Belongie, J. Hays, P. Perona, D. Ramanan, P. Dollár, and C. L. Zitnick. Microsoft coco: Common objects in context. *Computer Vision—ECCV 2014: 13th European Conference, Zurich, Switzerland, September 6-12, 2014, Proceedings, Part V 13*, 2014. ISSN 16113349. doi: 10.1007/978-3-319-10602-1_48.
- [25] Z. Lin, X. Peng, P. Cong, Y. Hou, X. Zhu, S. Yang, and Y. Ma. Wildrefer: 3d object localization in large-scale dynamic scenes with multi-modal visual data and natural language. *arXiv preprint arXiv:2304.05645*, 2023.
- [26] H. Liu, A. Lin, X. Han, L. Yang, Y. Yu, and S. Cui. Refer-it-in-rgb: A bottom-up approach for 3d visual grounding in rgb images. *Proceedings of the IEEE Computer Society Conference on Computer Vision and Pattern Recognition*, 2021. ISSN 10636919. doi: 10.1109/CVPR46437.2021.00597.
- [27] Y. Liu, M. Ott, N. Goyal, J. Du, M. Joshi, D. Chen, O. Levy, M. Lewis, L. Zettlemoyer, and V. Stoyanov. Roberta: A robustly optimized bert pretraining approach. *arXiv preprint arXiv:1907.11692*, 2019.
- [28] Z. Liu, Z. Zhang, Y. Cao, H. Hu, and X. Tong. Group-free 3d object detection via transformers. *Proceedings of the IEEE International Conference on Computer Vision*, 2021. ISSN 15505499. doi: 10.1109/ICCV48922.2021.00294.
- [29] J. Luo, J. Fu, X. Kong, C. Gao, H. Ren, H. Shen, H. Xia, and S. Liu. 3d-sps: Single-stage 3d visual grounding via referred point progressive selection. *Proceedings of the IEEE Computer Society Conference on Computer Vision and Pattern Recognition*, 2022-June, 2022. ISSN 10636919. doi: 10.1109/CVPR52688.2022.01596.
- [30] T. Miyanishi, F. Kitamori, S. Kurita, J. Lee, M. Kawanabe, and N. Inoue. Cityrefer: Geography-aware 3d visual grounding dataset on city-scale point cloud data. *Thirty-seventh Conference on Neural Information Processing Systems Datasets and Benchmarks Track*, 2023.
- [31] K. B. Park, M. Kim, S. H. Choi, and J. Y. Lee. Deep learning-based smart task assistance in wearable augmented reality. *Robotics and Computer-Integrated Manufacturing*, 63, 2020. ISSN 07365845. doi: 10.1016/j.rcim.2019.101887.
- [32] Y. Pei, X. Zhao, H. Li, J. Ma, J. Zhang, and S. Pu. Clusterformer: Cluster-based transformer for 3d object detection in point clouds. *Proceedings of the IEEE/CVF International Conference on Computer Vision*, 2024. ISSN 15505499. doi: 10.1109/iccv51070.2023.00613.
- [33] M. Prabhudesai, H. Y. F. Tung, S. A. Javed, M. Sieb, A. W. Harley, and K. Fragkiadaki. Embodied language grounding with 3d visual feature representations. *Proceedings of the IEEE Computer Society Conference on Computer Vision and Pattern Recognition*, 2020. ISSN 10636919. doi: 10.1109/CVPR42600.2020.00229.

- [34] X. Puig, K. Ra, M. Boben, J. Li, T. Wang, S. Fidler, and A. Torralba. Virtualhome: Simulating household activities via programs. *Proceedings of the IEEE Computer Society Conference on Computer Vision and Pattern Recognition*, 2018. ISSN 10636919. doi: 10.1109/CVPR.2018.00886.
- [35] S. Shi, C. Guo, L. Jiang, Z. Wang, J. Shi, X. Wang, and H. Li. Pv-rcnn: Point-voxel feature set abstraction for 3d object detection. *Proceedings of the IEEE Computer Society Conference on Computer Vision and Pattern Recognition*, 2020. ISSN 10636919. doi: 10.1109/CVPR42600.2020.01054.
- [36] P. Sun, H. Kretzschmar, X. Dotiwalla, A. Chouard, V. Patnaik, P. Tsui, J. Guo, Y. Zhou, Y. Chai, B. Caine, V. Vasudevan, W. Han, J. Ngiam, H. Zhao, A. Timofeev, S. Ettinger, M. Krivokon, A. Gao, A. Joshi, Y. Zhang, J. Shlens, Z. Chen, and D. Anguelov. Scalability in perception for autonomous driving: Waymo open dataset. *Proceedings of the IEEE Computer Society Conference on Computer Vision and Pattern Recognition*, 2020. ISSN 10636919. doi: 10.1109/CVPR42600.2020.00252.
- [37] A. Vaswani, N. Shazeer, N. Parmar, J. Uszkoreit, L. Jones, A. N. Gomez, Łukasz Kaiser, and I. Polosukhin. Attention is all you need. *Advances in neural information processing systems*, 30, 2017.
- [38] Z. Wang, H. Huang, Y. Zhao, L. Li, X. Cheng, Y. Zhu, A. Yin, and Z. Zhao. 3drp-net: 3d relative position-aware network for 3d visual grounding. *EMNLP 2023 - 2023 Conference on Empirical Methods in Natural Language Processing, Proceedings*, 2023. doi: 10.18653/v1/2023.emnlp-main.656.
- [39] E. Wijmans, S. Datta, O. Maksymets, A. Das, G. Gkioxari, S. Lee, I. Essa, D. Parikh, and D. Batra. Embodied question answering in photorealistic environments with point cloud perception. *Proceedings of the IEEE Computer Society Conference on Computer Vision and Pattern Recognition*, 2019-June, 2019. ISSN 10636919. doi: 10.1109/CVPR.2019.00682.
- [40] D. Wu, W. Han, T. Wang, Y. Liu, X. Zhang, and J. Shen. Language prompt for autonomous driving. *arXiv preprint arXiv:2309.04379*, 2023.
- [41] Y. Wu, X. Cheng, R. Zhang, Z. Cheng, and J. Zhang. Eda: Explicit text-decoupling and dense alignment for 3d visual grounding. *Proceedings of the IEEE/CVF Conference on Computer Vision and Pattern Recognition*, pages 19231–19242, 2023.
- [42] Y. Yan, Y. Mao, and B. Li. Second: Sparsely embedded convolutional detection. *Sensors (Switzerland)*, 18, 2018. ISSN 14248220. doi: 10.3390/s18103337.
- [43] L. Yang, Z. Zhang, Z. Qi, Y. Xu, W. Liu, Y. Shan, B. Li, W. Yang, P. Li, Y. Wang, et al. Exploiting contextual objects and relations for 3d visual grounding. *Advances in Neural Information Processing Systems*, 36, 2024.
- [44] Z. Yang, S. Zhang, L. Wang, and J. Luo. Sat: 2d semantics assisted training for 3d visual grounding. *Proceedings of the IEEE International Conference on Computer Vision*, 2021. ISSN 15505499. doi: 10.1109/ICCV48922.2021.00187.
- [45] T. Yin, X. Zhou, and P. Krahenbuhl. Center-based 3d object detection and tracking. *Proceedings of the IEEE/CVF conference on computer vision and pattern recognition*, pages 11784–11793, 2021.
- [46] Z. Yuan, X. Yan, Y. Liao, R. Zhang, S. Wang, Z. Li, and S. Cui. Instancerefer: Cooperative holistic understanding for visual grounding on point clouds through instance multi-level contextual referring. *Proceedings of the IEEE International Conference on Computer Vision*, 2021. ISSN 15505499. doi: 10.1109/ICCV48922.2021.00181.
- [47] Z. Yuan, X. Yan, Z. Li, X. Li, Y. Guo, S. Cui, and Z. Li. Toward explainable and fine-grained 3d grounding through referring textual phrases. *arXiv preprint arXiv:2207.01821*, 2022.
- [48] Y. Zhan, Y. Yuan, and Z. Xiong. Mono3dvg: 3d visual grounding in monocular images. *Proceedings of the AAAI Conference on Artificial Intelligence*, 38(7):6988–6996, 2024.

- [49] Y. Zhang, Z. M. Gong, and A. X. Chang. Multi3drefer: Grounding text description to multiple 3d objects. *Proceedings of the IEEE International Conference on Computer Vision*, 2023. ISSN 15505499. doi: 10.1109/ICCV51070.2023.01397.
- [50] L. Zhao, D. Cai, L. Sheng, and D. Xu. 3dvg-transformer: Relation modeling for visual grounding on point clouds. *Proceedings of the IEEE International Conference on Computer Vision*, 2021. ISSN 15505499. doi: 10.1109/ICCV48922.2021.00292.
- [51] Z. Zhou, X. Zhao, Y. Wang, P. Wang, and H. Foroosh. Centerformer: Center-based transformer for 3d object detection. *European Conference on Computer Vision*, 13698 LNCS, 2022. ISSN 16113349. doi: 10.1007/978-3-031-19839-7_29.
- [52] B. Zhu, Z. Jiang, X. Zhou, Z. Li, and G. Yu. Class-balanced grouping and sampling for point cloud 3d object detection. *arXiv preprint arXiv:1908.09492*, 2019.

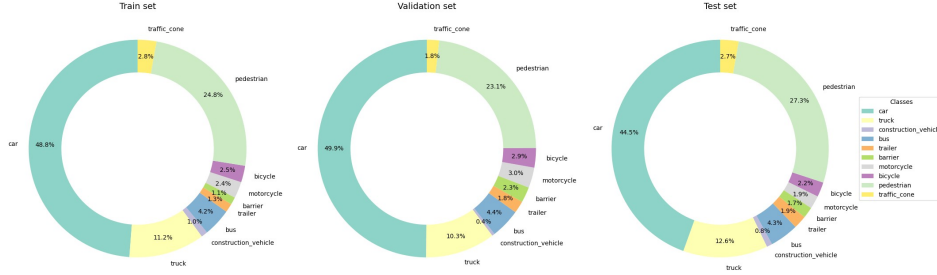


Figure 4: Talk2Car-3D dataset statistics on train, validation, and test sets.

A Appendix

This supplementary material provides comprehensive additional information to support and extend the main paper. **Section A** describes data preprocessing and statistics of Talk2car-3D. **Section B** presents the implementation details of our training process, thoroughly explaining technical aspects. **Section C** provides extensive experimental analysis, while **Section D** discusses the current limitations and future research.

A.1 Dataset

Based on Talk2Car [10], originally introduced as a 2D visual grounding dataset, we construct Talk2car-3D following MSSG’s preprocessing [9] approach to extend its applicability to 3D scenarios. We refine the target objects from Talk2Car for our training and inference based on three criteria: (1) inclusion in the 10 super categories covered in the nuScenes object detection task, (2) presence within the detection range specific to each category in nuScenes, and (3) containment of at least one point in their ground-truth 3D bounding boxes. This process yields 7,115 training, 998 validation, and 2,056 test commands. For each scenario, we utilize visual data consisting of point clouds from 10 sweeps and their corresponding image, following nuScenes protocol. As shown in Fig. 4, Talk2Car-3D exhibits category imbalance across all data splits. We perform an in-depth analysis of individual categories in **Section C**.

A.2 Implementation Details

We train LidaRefer for 20 epochs with a batch size of 4 on 4 Nvidia A6000 GPUs. Adam [22] optimizer using a one-cycle policy is used with a maximum learning rate of $4e-4$, a weight decay of 0.01, and a momentum from 0.85 to 0.95. The layers for the encoder and decoder are $N_E = 1$ and $N_D = 3$, respectively, while the numbers of visual tokens (i.e., selected foreground features) and decoder’s queries are 500 and 256, respectively. The detection range is $[-54, 54]m$, $[0, 54]m$ and $[-5, 3]m$ for the X, Y, and Z-axes, respectively, and the voxel size is $(0.075m, 0.075m, 0.2m)$.

During training our networks (i.e., heatmap head, target identification network, and decoder), we employ a center-based object detector’s assignment strategy [45, 51]. This strategy constrains each network to learn information exclusively about objects whose centers align with the positions of the selected features. To achieve stable and faster convergence of training, we manually select features necessary for subsequent modules during the foreground feature selection and query proposal generation stages. Specifically, in the foreground feature selection, we first ensure selected foreground features \mathcal{F}_V retain information about all objects within a scene by manually incorporating the features from \mathcal{F}_{BEV} that are positioned at the central locations of all objects into \mathcal{F}_V . Then, the remaining features of \mathcal{F}_V are chosen based on the heatmap scores predicted by the model from \mathcal{F}_{BEV} . Likewise, in the query proposal generation, we ensure queries \mathcal{Q} retain information about the target object by manually incorporating the feature positioned at the central location of the target.

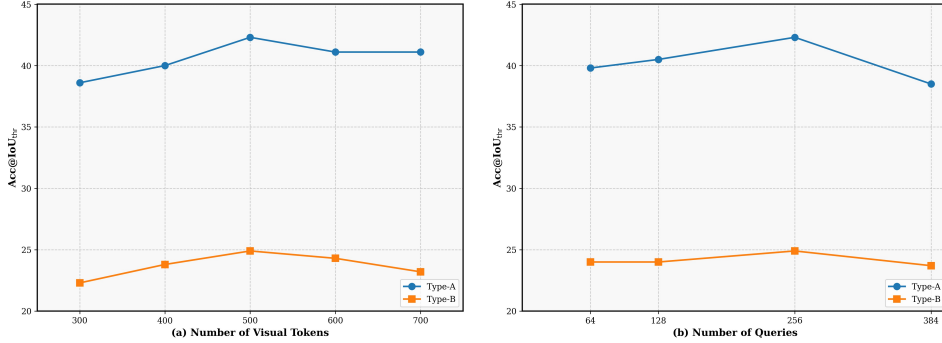


Figure 5: Performance comparison of varying the number of visual tokens and queries on Talk2Car-3D validation set

Table 6: Per-category performance in Type-A for the 10 categories on the Talk2Car-3D validation and test sets.

Method	Car	Truck	C.V.	Bus	Trailer	Barrier	Motorcycle	Bicycle	Pedestrian	T.C.	Total
<i>Validation set</i>											
MSSG-Re	33.6	22.3	25.0	29.5	5.5	0	46.7	34.5	40.0	33.3	32.8
LidaRefer-B	41.0	35.9	25.0	29.5	33.3	21.7	60.0	37.9	50.9	50.0	42.3
<i>Test set</i>											
MSSG-Re	34.5	25.9	5.9	39.8	0	8.8	60.0	20.0	46.3	25.0	35.5
LidaRefer-B	41.1	32.4	29.4	38.6	27.5	20.6	50.0	22.2	56.4	39.4	43.1

A.3 Additional Analysis

A.3.1 Sizes of Visual Tokens and Queries

Fig. 5 examines the impact of varying the number of visual tokens and decoder’s queries. It shows that neither reducing nor increasing the number of visual tokens and queries necessarily leads to performance improvements.

Specifically, we observe that the number of visual tokens plays an important role in performance, as in Fig. 5(a). We hypothesize that insufficient visual tokens may fail to provide adequate visual information for capturing contextual details. Conversely, even with our foreground feature selection method, selecting too many features beyond the optimal range might introduce irrelevant visual information from dominant background points and empty spaces. This extraneous information could hinder cross-modal alignment, negatively affecting the model’s overall performance.

Similarly, the number of queries significantly affects performance, as in Fig. 5(b). We believe that an insufficient number of queries might limit the ability to capture of the in-formation of non-target objects in spatial relationships with the target object during our localization method. Conversely, selecting too many queries beyond the optimal range might introduce information about non-target objects irrelevant to target identification, potentially complicating learning meaningful spatial relationships.

A.3.2 Per-Category Performance

Table 6 compares the per-category performance on Talk2Car-3D validation and test sets, respectively, in Type-A. LidaRefer achieves the best performance across all categories in the validation set and in 8 out of 10 categories in the test set. Notably, significant improvements are observed in minor categories, despite these categories appearing as targets in only 10% of the training set. It shows that our foreground feature selection and ambiguous object localization effectively incorporate and learn from non-target object information during training, leading to a deeper understanding of minor categories. This comprehensive learning approach improves robustness across all categories, even those with limited representation as targets in the training data.

A.4 Limitation and Future Works

Although LidaRefer achieves SOTA performance, we perform relatively implicit cross-modal feature alignment relying on transformer-based networks. Recently, methods such as MDETR [21], BUTD-DETR [20], and EDA [41] have tried to devise explicit cross-modal feature alignment through contrastive learning. In the future, we plan to apply these techniques to LidaRefer to achieve more explicit cross-modal feature alignment as a way of enhancing its generalization ability and extending its applications.